Energy Storage Materials 15 (2018) 388–395

Contents lists available at ScienceDirect

Energy Storage Materials

journal homepage: www.elsevier.com/locate/ensm

A flexible carbon/sulfur-cellulose core-shell structure for advanced lithium–sulfur batteries

Lu Li[a,1], Lijuan Hou[b,c,1], Jie Cheng[a,1], Trevor Simmons[c], Fuming Zhang[c], Lucy T. Zhang[a], Robert J. Linhardt[c,*], Nikhil Koratkar[a,d,**]

[a] Department of Mechanical, Aerospace and Nuclear Engineering, Rensselaer Polytechnic Institute, 110 8th Street, Troy, NY 12180, USA
[b] Center for Nanoscience and Nanotechnology, Zhejiang Sci-Tech University, 5 Second Avenue, Xiasha Higher Education Zone, Hangzhou 310018, PR China
[c] Departments of Chemistry and Chemical Biology, Chemical and Biological Engineering, Biology and Biomedical Engineering, Center for Biotechnology and Interdisciplinary Studies, Rensselaer Polytechnic Institute, 110 8th Street, Troy, NY 12180, USA
[d] Department of Materials Science and Engineering, Rensselaer Polytechnic Institute, 110 8th Street, Troy, NY 12180, USA

A B S T R A C T

Lithium sulfur (Li-S) batteries are viewed as a promising candidate for next-generation energy storage systems due to their high energy density, low cost and ease of manufacturing. However, rapid capacity decay caused by lithium polysulfide shuttle during charging/discharging processes hinder its practical application. In this work, we demonstrate a cellulose encapsulated carbon/sulfur core-shell structure for advanced Li-S batteries based on electrostatic spinning with coaxial spinnerets. Cellulose serves as an excellent "shell" due to its good ion conductivity, flexible structure to accommodate volumetric expansion of sulfur, and strong capability to prevent sulfur and its intermediate reaction products from dissolving into the electrolyte. CMK-3 mesoporous carbon in the core is helpful to confine sulfur in the pores, and improve the electrical conductivity of the fiber electrode together with the carbon black particles on the outside of the fiber. As a result, the obtained cellulose based flexible sulfur electrode delivers a high initial discharge capacity (> 1200 mA h g^{-1}), good electrochemical performance with Coulombic efficiency above 99%, and a low capacity decay rate of ~ 0.12% per cycle over 300 charging/discharging cycles.

1. Introduction

Lithium–sulfur (Li–S) battery is a rechargeable battery chemistry that utilizes sulfur as cathode and lithium as anode. Li-S battery is viewed as a promising next generation battery technology due to its high theoretical energy density of ~ 2675 W h kg^{-1} (or ~ 2800 W h L^{-1}), which is about 5 times greater than that of state-of-art Lithium-ion batteries (LIBs) [1]. Besides, sulfur is low-cost, abundant and environmental friendly, unlike the current electrode materials employed in LIBs such as lithium cobalt oxide and lithium manganese oxide. However, a series of technical challenges have constrained the commercialization of Li–S battery. As an electrode material, sulfur must overcome its insulating nature. The dissolution of intermediate lithium polysulfides in organic liquid electrolytes during charge/discharge also leads to low utilization of sulfur and a fast capacity decay. Besides, a large volumetric expansion would accompany the discharge process which can cause structural damage to the electrode [2,3].

Extensive research has been conducted to address these challenges. For example, adopting chemical immobilizers (chemically functionalized groups [4–6], two dimensional materials (such as ReS_2, MoS_2 and phosphorene) [7–9], phosphides [10], oxides [11], hydroxide materials [12] and copolymer framework [13] to bond lithium polysulfides, or confining sulfur spatially inside conductive and deformable nanostructures, such as porous carbon/metal oxide spheres [14–16] or nanowires/nanotubes have been explored [17]. However, most of the work adopted an "outside-in" approach to confine sulfur in these unique nanostructures, which first requires fabrication of these structures and then infiltration of molten sulfur or dissolved sulfur. However, it is inevitable that there will be residual sulfur remaining outside. Therefore, a post heating method has to be used to eliminate the residual sulfur covering the outer surface of the hosts [18]. In contrast, an "inside-out" approach could avoid the issue of residual sulfur. However, this type of strategy is also challenging to realize due to significant sulfur loss (low melting and boiling temperature of sulfur)

* Corresponding author.
** Corresponding author at: Department of Mechanical, Aerospace and Nuclear Engineering, Rensselaer Polytechnic Institute, 110 8th Street, Troy, NY 12180, USA.
E-mail addresses: linhar@rpi.edu (R.J. Linhardt), koratn@rpi.edu (N. Koratkar).
[1] These authors contributed equally in this manuscript.

https://doi.org/10.1016/j.ensm.2018.08.019
Received 20 April 2018; Received in revised form 20 August 2018; Accepted 21 August 2018
Available online 23 August 2018

during the fabrication processes of these nanostructures.

Polymer materials have been widely used for applications such as energy storage [13,19] and drug delivery [20]. They could be used to encapsulate and controllably release desired chemicals due to the internal pore space within the polymer matrix which could be used to transport ions, such as lithium ions [17]. Due to their soft nature, polymers can also be used as a container to accommodate the large volume change during charge and discharge. For example, polymer coatings have been used to withstand the ~ 400% volume expansion of silicon on lithiation [21]. Cellulose is the most abundant biopolymer on earth and is found in the cell walls of plants or made by bacteria. As a biocompatible polymer, it has been widely applied in battery systems, such as the separator to replace polyolefins (made from the ever-decreasing fossil oil) [22] as well as the binder to replace polyvinylidene difluoride (which requires the use of volatile and toxic solvents for processing) [23]. In addition, cellulose can be used to make fibers with high tensile strength because of its highly crystalline linear structure and then be fabricated into different shapes.

In this paper, we report an inside-out method to synthesize fiber-based sulfur electrodes for high performance lithium sulfur batteries. The key point of our design is to introduce cellulose for sulfur encapsulation using electrostatic spinning with coaxial spinnerets, which facilitates the production of core-shell fibers. The resulting fiber electrode has a cellulose shell and a CMK-3/S (carbon/sulfur) composite as the core. Carbon black particles, decorated on the outside the cellulose, are introduced during the solidifying process of the fiber. The cellulose shell has very good ion conductivity and a strong capacity to accommodate volumetric expansion. In addition, after encapsulating sulfur, cellulose can prevent sulfur and its intermediate reaction products, such as lithium polysulfides, from being washed away, therefore limiting its dissolution and migration during discharge/charge processes. Here the CMK-3 mesoporous carbon in the core can also help to confine sulfur, while improving the conductivity of the fiber electrode together with the carbon black particles on the outside of the fiber. The resulting Cellulose(CMK-3/S)CB freestanding electrode can deliver a high discharge capacity above 1200 mA h g^{-1}. After 300 cycles of discharge and charge, the reversible capacity of the Cellulose(CMK-3/S)CB freestanding electrode remains at around 660 mA h g^{-1} with a Coulombic efficiency above 99%, and a low capacity decay rate of ~ 0.12% per cycle.

2. Experimental section

2.1. Synthesis of CMK-3/S composite

Commercial sulfur (Alfa Aesar) was impregnated into CMK-3 mesoporous carbon (ACS Material) by mixing (weight ratio of 3:1) and heating to ~ 155 °C for several hours.

2.2. Synthesis of Cellulose(CMK-3/S)CB fiber

Cellulose (Weyerhaeuser Co.) was added to room temperature ionic liquid (RTIL) 1-ethyl-3-methylimidazolium acetate ([EMIM][Ac]) to prepare a 2%(w/v) cellulose sheath solution. Core solution is made of 20%(w/v) CMK-3/S composite dispersed in triton-x 100 (Sigma-Aldrich). The mixtures were mechanically stirred by using magnetic stirrer (Fisher Scientific) at ~ 80 °C until the homogeneous solutions were formed. Then these solutions were placed into a 10 mL syringe and connected to the spinneret (MECC, Ogori, Fukuoka, Japan). Cellulose(CMK-3/S) core-sheath fibers were fabricated by using a co-electrospinning process with a coaxial spinneret. The diameter of the inner needle and outer needle were ~ 0.94 mm and ~ 2.50 mm, respectively. The distance between the spinneret tip and aluminum collector electrode was fixed at ~ 15 cm. Total flow rate (core: ~ 120 μL/min and sheath: ~ 180 μL/min, fed at a constant rate by using the mechanical syringe pump (NE-1000, New Era Pump System Inc.)) and applied voltage (~ 15 kV) were optimized to obtain good electrospinnability. Electrospun fibers were collected into a coagulation bath, which was filled with a 2%(w/v) carbon black (CB) particles dispersed in a water/ethanol mixture to remove the ionic liquid thereby solidifying the fibers, while also coating carbon black particles on the outside surfaces of the fibers. The fibers (Cellulose(CMK-3/S)CB) formed an entangled web (fiber mat) in the coagulation bath and were subsequently removed, washed and freeze-dried under vacuum. Pure cellulose electrospun fibers were also fabricated by using a single spinneret and a coagulation bath without carbon black particles.

2.3. Electrochemical testing

Electrochemical experiments were performed by using 2032-type coin cells, which were assembled in an argon-filled glove box. The freestanding electrode was cut from the Cellulose(CMK-3/S)CB fiber mat directly. No binder, conductive additive and current collector were used. For comparison, the CMK-3/S electrode was fabricated by a homogeneous slurry (60 wt% CMK-3/S as the active material, 5 wt% carbon black as the conductive agent and 35 wt% PVDF as the binder (in order to keep similar sulfur content and conductive carbon content) dissolved in N-methyl-2-pyrrolidone (NMP)), which was spread on Al foil by using a doctor blade. The electrolyte was a mixture of 1 M lithium bis(trifluoromethanesulfonyl)imide in 1,3-dioxolane and 1,2-dimethoxyethane (1:1 by volume) with a 0.1 mol L^{-1} $LiNO_3$ additive. The specific capacities were calculated using the weight of sulfur. An Arbin BT2000 battery instrument was used to perform galvanostatic charge–discharge cycles at various current densities over the voltage range from 1.5 to 2.8 V (vs. Li/Li^+). Cyclic voltammetry (CV) measurements and electrochemical impedance spectroscopy (EIS) were carried out by using a Gamry Instruments potentiostat at a scan rate of 0.2 mV s^{-1} in the voltage range of 1.5–2.8 V (vs. Li^+/Li) and in the frequency range of 1 MHz to 100 mHz at room temperature.

2.4. Material characterization

The morphology and structure of the materials were investigated by using a field emission scanning electron microscope (SEM) FEI-VERSA. The transmission electron microscopy (TEM) images were obtained by depositing electrospun fibers onto 400 mesh copper grids and performed with a JEOL JEM-2011 TEM (JEOL Ltd., Tokyo, Japan) at an accelerating voltage of ~ 200 kV. Raman spectroscopy was performed by using a Witec Alpha 300R confocal Raman imaging system. X-ray diffraction (XRD) was performed by using a Bruker D8-DISCOVER with a Cu Kα radiation source and a pyrolytic graphite monochromator. Fourier transform infrared (FTIR) spectra were collected with a Varian 660-IR FTIR spectrophotometer (Varian Inc. USA). Thermogravimetric analysis was performed using a computer-controlled TA Instruments TGA Q50 apparatus under a nitrogen atmosphere at a heating rate of ~ 10 °C per min.

2.5. Linear elasticity simulation

The elastic deformation simulation is carried out with Abqus FEA software. In both cases, the length of the tubes is 300 nm, the inner diameter is 80 nm and the outer diameter is 100 nm. We assume the tubes are homogeneous and isotropic with linear elasticity. The volume change is restricted in the middle portion of the tube [24]. Young's modulus of the cellulose is taken as ~ 10 GPa, and Possion's ratio is ~ 0.3 [25,26]. Young's modulus of the carbon nanotube is taken as ~ 500 GPa with a Possion's ratio of 0.285 [27,28].

3. Result and discussion

The schematic illustration of the synthesis procedure for the Cellulose(CMK-3/S)CB composite is shown in Fig. 1a. With the use

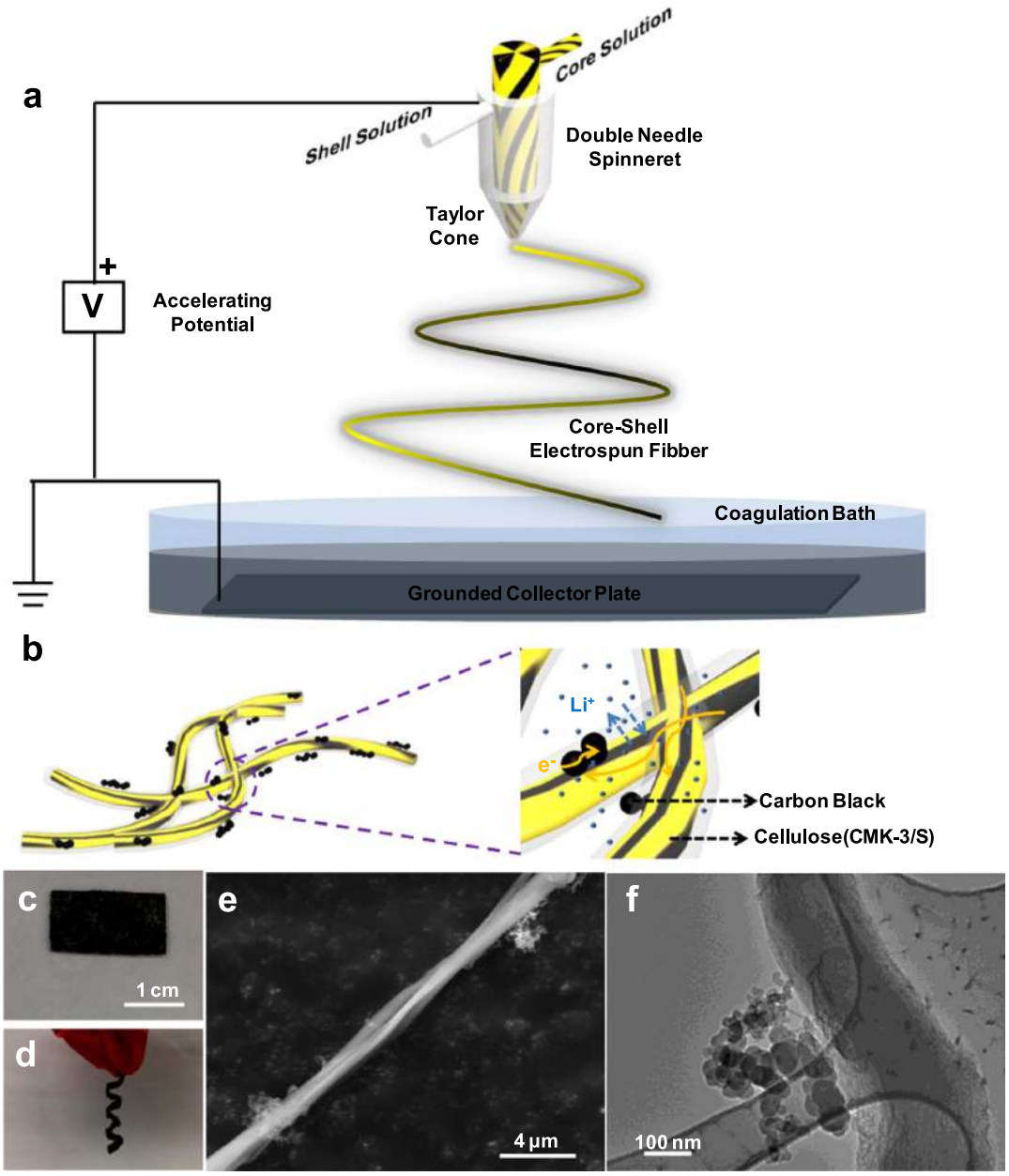

Fig. 1. (**a**, **b**) Synthetic schemes for the preparation of Cellulose(CMK-3/S)CB composite. (**c**, **d**) Digital photographs of Cellulose(CMK-3/S)CB composites. (**e**) SEM and (**f**) TEM images of Cellulose(CMK-3/S)CB composite.

of coaxial and multiaxial spinnerets, core-shell fibers could be easily produced. Here we employ the RTIL as the solvent to dissolve the cellulose as the shell material, and Triton X-100 surfactant to disperse CMK-3/S composite, which has been encapsulated in the core. Electrospun Cellulose(CMK-3/S) fibers were collected into a coagulation bath, which was filled with a water/ethanol mixture containing carbon black particles. Electrospun cellulose fibers have been positively charged, which could attract and absorb carbon black particles. The coagulation bath plays a dual role during the fabrication process. First, the coagulation bath removes RTIL, thereby solidifying the fibers. Second, it facilitates the coating of carbon black particles on the outside surfaces of the fibers (Fig. 1b) to obtain the Cellulose(CMK-3/S)CB composite. In addition, the pure electrospun cellulose fibers were also collected in the water/ethanol mixture coagulation bath to remove RTIL and solidify the fibers. The pure cellulose and Cellulose(CMK-3/S)CB fibers were then washed extensively with distilled water to remove fiber fragments and loosely bound carbon black particles. After freeze drying, we obtained a “cotton ball” like fiber mesh that could be made into different shapes, such as square and heliciform as shown in Fig. 1c, d. Pure cellulose electrospun fiber was white in color, while after incorporating CMK-3/S composite and carbon black, the fiber turned black. Scanning electron microscope (SEM) was carried out to characterize these fibers. It can be seen that the pure fiber has a very clean surface and solid structure (Supporting information, Fig. S1), while the surface of Cellulose(CMK-3/S)CB fiber has been decorated with clusters of carbon black particles (Fig. 1e). Transmission electron microscopy (TEM) image (Fig. 1f) further confirms the obtained Cellulose(CMK-3/S)CB fiber has a well-defined

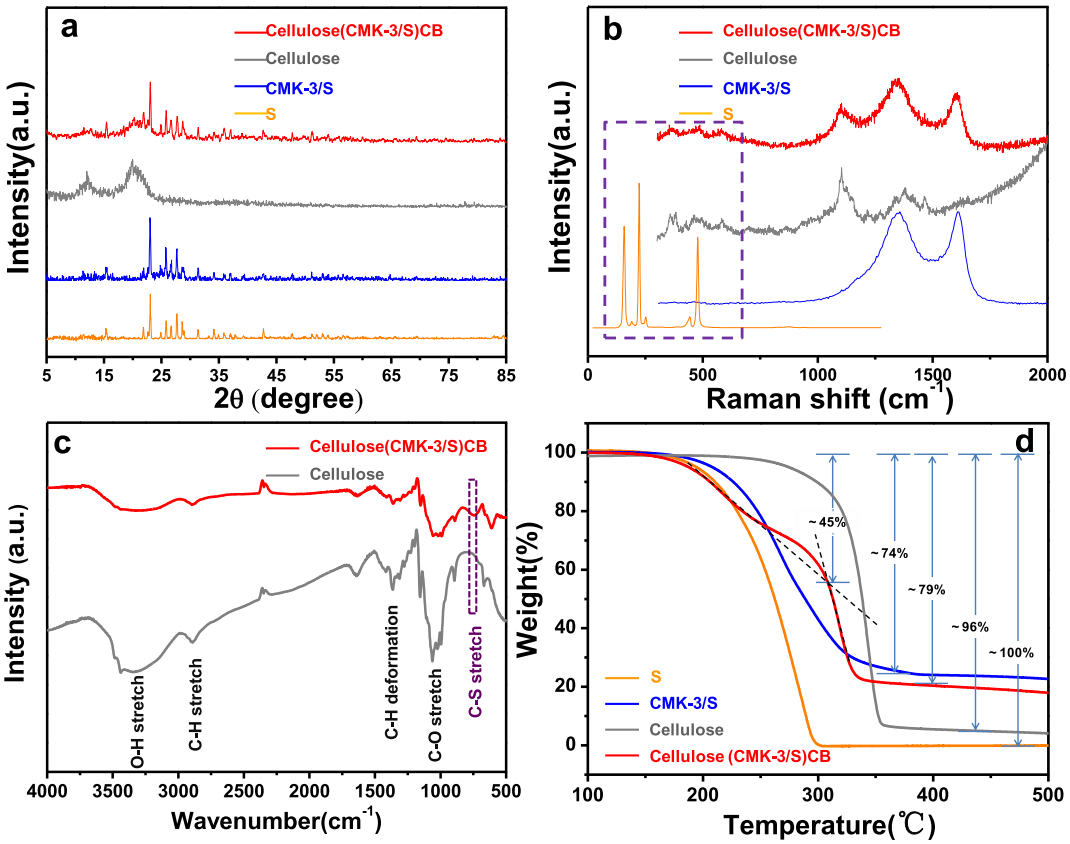

Fig. 2. (**a**) XRD patterns and (**b**) Raman spectra of the Cellulose(CMK-3/S)CB, Cellulose, CMK-3/S and commercial S samples. (**c**) FTIR spectra of the Cellulose(CMK-3/S)CB composite and Cellulose. (**d**) TGA results of the Cellulose(CMK-3/S)CB, Cellulose, CMK-3/S and commercial S samples.

core-shell structure.

Fig. 2a shows the X-ray diffraction (XRD) patterns of the Cellulose(CMK-3/S)CB, Cellulose, CMK-3/S and commercial S samples. In the spectrum of Cellulose(CMK-3/S)CB and Cellulose, we observe two characteristic peaks of cellulose [29,30]. The diffraction peaks of CMK-3/S sample could be mainly designated to sulfur. After cellulose wrapping of the CMK-3/S composite and decoration with the carbon black, there are no significant differences in the XRD patterns of the CMK-3/S and Cellulose(CMK-3/S)CB composites, except for the two characteristic peaks of cellulose, indicating that the electrospinning process did not induce any structural changes to the CMK-3/S composite. However, the intensities of sulfur peaks weakened indicating that the sulfur was highly dispersed inside these composite materials. In order to study the interaction between the CMK-3/S composite, cellulose and carbon black, Raman information is presented in the Fig. 2b. Peaks observed at around 1350 cm^{-1} and 1590 cm^{-1} are assigned to the D band (correspond to disordered/defective graphitic structures) and G band (attributed to the tangential vibration of the carbon atoms) of carbon based materials [31]. The bands at about 1100 cm^{-1} and 1380 cm^{-1} from the spectrum are characteristic bands from cellulose [32], and one peak at around 1100 cm^{-1} could be observed clearly in the Cellulose(CMK-3/S)CB composite, while another peak at around 1380 cm^{-1} overlaps with the D band of CMK-3 and carbon black. Sulfur bands mainly concentrated at the Raman shifts below 500 cm^{-1}. However, these bands could not be observed when the sulfur was combined with CMK-3, suggesting that the sulfur has been impregnated into the mesoporous carbon matrix [33]. The intensity ratio of D band and G band (I_D/I_G) could be used to evaluate the defects present in carbon nanomaterials. The value of I_D/I_G has increased from 0.94 (CMK-3) to 1.02 (CMK-3/S), which also indicates that sulfur has generated more disordered graphitic structures through deformation of the sp^2 carbon lattice (Supporting information, Fig. S2) [34]. From the FTIR spectra (Fig. 2c), the absorption band at around 3300 cm^{-1} is assigned to hydroxyl groups (O-H) stretching. Bands at around 2885 cm^{-1} and 1365 cm^{-1} are assigned to stretching and deformation vibrations of C-H group. The band at about 1060 cm^{-1} is assigned to -C-O- group [35]. Note that the C-S stretch (at about 746 cm^{-1}) also appear in the spectrum of Cellulose(CMK-3/S)CB composite [36], which confirms the existence of sulfur in the Cellulose(CMK-3/S)CB composite. The hydroxyl groups in cellulose could also stabilize sulfur/polysulfide species, which will contribute to the superior stability of the Li-S battery with Cellulose(CMK-3/S)CB electrode [37]. Sulfur content in the Cellulose(CMK-3/S)CB composite and CMK-3/S composite were measured by thermogravimetric analysis (TGA, Fig. 2d). According to the measurement, the decomposition temperature of the CMK-3/S sample was around 160 °C and the S content was ~ 75 wt%. The amount of sulfur loading in the Cellulose(CMK-3/S)CB composite is calculated to be ~ 45 wt% in the composite and the decomposition temperature of electrospun cellulose nanofibers was around 300 °C. It should be noted that after wrapping of sulfur into the core of cellulose nanofibers, the sublimation rate of sulfur has been reduced compared to the thermo-gravimetric curves of commercial bulk sulfur and CMK-3/S composite, which suggested that sulfur was confined and more stable in this core-shell structure.

Cyclic voltammetry (CV, here we demonstrated the second cycle of CV scans due to the electrochemical activation existing in the first CV cycle) was used to study the reaction kinetics of Li-S battery with the Cellulose(CMK-3/S)CB freestanding electrode and CMK-3/S electrode (Fig. 3a). Two reduction peaks could be observed in both electrode materials. The peaks at around 2.20 V and 2.00 V corresponded to the

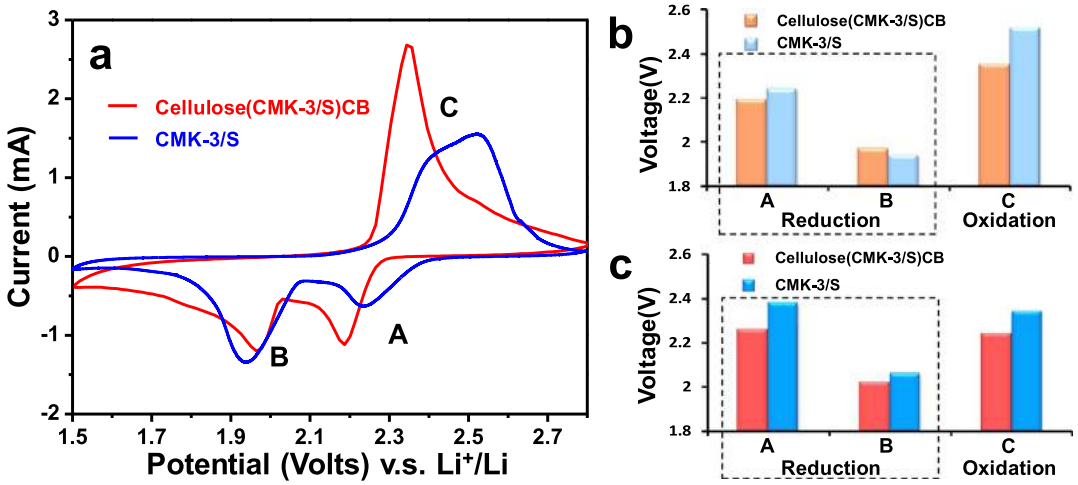

Fig. 3. (**a**) CV plots of Li-S batteries with the Cellulose(CMK-3/S)CB freestanding electrode and CMK-3/S electrode. (**b–c**) Comparison of the peak potentials and onset potentials of the Cellulose(CMK-3/S)CB freestanding electrode and CMK-3/S electrode during the redox process.

two-step conversions of sulfur into high-order lithium polysulfides (Li_2S_x, $4 \le x \le 8$) and high-order lithium polysulfides into Li_2S_2/Li_2S, respectively. In the oxidation process, one merged peak could be observed, which suggested lithium sulfides (Li_2S_2/Li_2S) converted back to soluble lithium polysulfides (Li_2S_x, $4 \le x \le 8$) and then finally to sulfur [7]. We further analyzed the peak-potential (Fig. 3b) and onset-potential (derived by using the tangent method [38], Fig. 3c) obtained using CV. For the first reduction process (sulfur reduced into high-order lithium polysulfides), the onset-potential (2.26 V) and peak-potential (2.19 V) of Li-S battery with the Cellulose(CMK-3/S)CB freestanding electrode is smaller than those of Li-S battery with CMK-3/S electrode (2.38 V and 2.24 V), which indicates a reaction lag in the battery with the Cellulose(CMK-3/S)CB freestanding electrode. This is mainly due to the fact that the CMK-3/S composite has been encapsulated in the core structure of cellulose instead of being exposed to the electrolyte as the CMK-3/S electrode. It therefore takes some time for the electrolyte to pass through the internal surfaces of the cellulose shell, and hence the lag [17]. With respect to the oxidation reaction, onset-potential (2.24 V) and peak-potential (2.35 V) of the battery with the Cellulose(CMK-3/S)CB freestanding electrode are smaller compared to those with the CMK-3/S electrode (2.34 V and 2.52 V respectively). At the same time, the slopes of Tafel plots (Supporting information, Fig. S3) in the reduction and oxidation reaction do not show an obvious change, indicating that sulfur redox mechanisms still remain the same [39]. Therefore, the presence of cellulose does not affect the sulfur lithiation/delithiation reaction mechanisms. We have also increased CV scans of batteries with Cellulose(CMK-3/S)CB freestanding electrode and CMK-3/S electrode as shown in Fig. S4. For the battery with Cellulose(CMK-3/S)CB freestanding electrode, from the second cycle, the main reduction peaks and oxidation peak position remains almost unchanged and CV curves exhibit similar shapes, indicating the good reversibility. While for the CMK-3/S electrode, the decrease of the peak intensity and integral areas from the second to the third cycle, indicate the presence of irreversible reactions.

Electrochemical impedance spectroscopy (EIS) was used to analyze the electrochemical reaction kinetics to confirm whether or not the Cellulose(CMK-3/S)CB structure could provide good electronic and ionic transport pathways. Nyquist plots of Li-S battery with Cellulose(CMK-3/S)CB electrode and CMK-3/S electrode are qualitatively similar (Fig. S5) with a typical semicircle in the high medium frequency region and an inclined line at low frequencies. Fitted resistance values for the equivalent circuit elements [40,41] are shown in Table S1. Due to existence of the cellulose shell, which wraps the active material (sulfur), the transport of electrons from cellulose to sulfur in the Cellulose(CMK-3/S)CB freestanding electrode (R_{int}: 23.48 Ω) is a little slower than the transport of electrons from the Al foil current collector to sulfur in the CMK-3/S electrode (R_{int}: 4.16 Ω). Besides, the cellulose shell also causes a slight increase in the interface resistance between the inner conductive agent (CMK-3) and the electrolyte.

The electrochemical performance of the Cellulose(CMK-3/S)CB freestanding electrode was studied by galvanostatic charge/discharge tests under different rates up to 3 C (1 C = 1675 mA g^{-1}). For the control, we used the CMK-3/S electrode. Fig. 4a shows the rate performance of the electrodes. Under low current conditions of 0.2 C, the Cellulose(CMK-3/S)CB freestanding electrode exhibits a discharge capacity of above 1200 mA h g^{-1}, while the CMK-3/S electrode shows a discharge capacity of ~ 1100 mA h g^{-1}. With the increase of the current rate, specific capacities of ~ 991, ~ 915, ~ 864, ~ 617 and ~ 435 mA h g^{-1} were obtained at ~ 0.5 C, ~ 0.8 C, ~ 1 C, ~ 2 C and ~ 3 C rates, respectively, indicating the reversible charge/discharge capability over a wide range of operating current densities. When the rate was brought back to ~ 1 C after high current density testing, the specific capacity of the Cellulose(CMK-3/S)CB electrode went back to ~ 878 mA h g^{-1}, which is close to the initial value (864 mA h g^{-1}) at 1 C current density, indicating a good reversibility. We noticed that the specific capacity of the CMK-3/S electrode (~ 509 mA h g^{-1}) is larger than that of the Cellulose(CMK-3/S)CB freestanding electrode at very high current density (e.g. 3 C). This is due to the slightly lower electrical conductivity of freestanding Cellulose(CMK-3/S)CB compared to the CMK-3/S electrode, as the cellulose shell only contributes to ionic conduction and not to electron conduction. Further, lithium ions can react with the active sulfur material directly in the CMK-3/S electrode without passing through the cellulose shell. The CV results (Fig. 3) have also verified this as the reaction kinetics lags in the battery with the Cellulose(CMK-3/S)CB freestanding electrode. The galvanostatic charge/discharge curves for the Cellulose(CMK-3/S)CB freestanding electrode are displayed in Fig. 4b. The typical two-stage discharge behavior corresponds to the reduction of sulfur into high-order lithium polysulfides (Li_2S_x, $4 \le x \le 8$) at the high plateau and the conversion of Li_2S_x ($3 \le x \le 8$) to Li_2S_2/Li_2S at the lower plateau [42], which agrees well with the CV results (Fig. 3a). Due to the increased over-potential with large kinetic barriers caused by the conduction mode of Cellulose(CMK-3/S)CB electrode and the porous electrode material (CMK-3 mesoporous carbon) [43], separations between the discharge plateaus and charge plateaus were enlarged with increased current density. The cycling performance of the battery with the

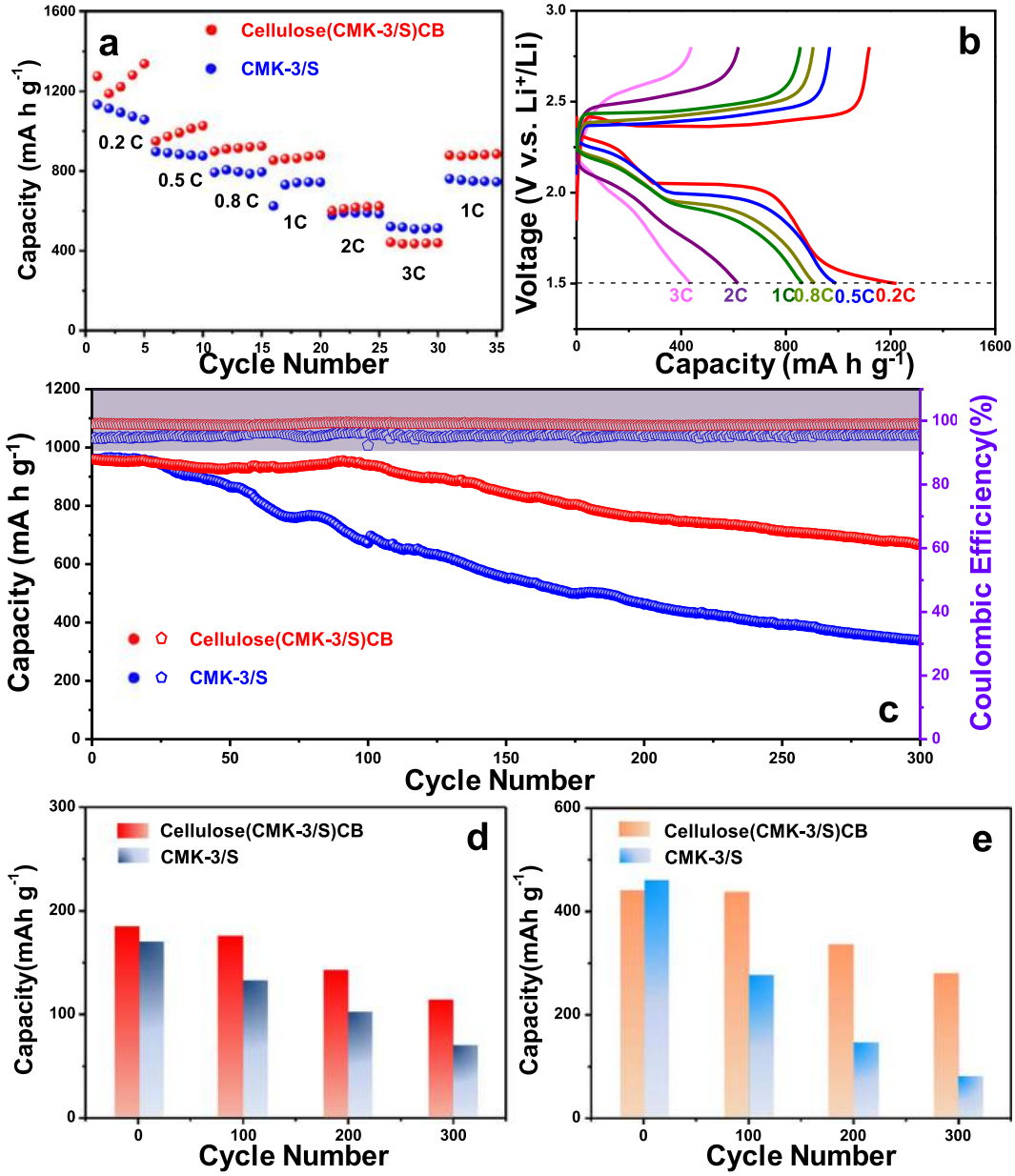

Fig. 4. Electrochemical properties of Li-S batteries with Cellulose(CMK-3/S)CB freestanding electrode and CMK-3/S electrode. (**a**) Rate properties at different current densities (1 C = 1675 mA g^{-1}). (**b**) Galvanostatic charge/discharge profiles of the third cycle under different rates within a potential window of 1.5–2.8 V vs. Li^+/Li for Li-S battery with the Cellulose(CMK-3/S)CB freestanding electrode. (**c**) Cycling stability and decay rate per cycle at a current density of 0.5 C. (**d**) High plateau and (**e**) low plateau discharge capacities for Cellulose(CMK-3/S)CB and CMK-3/S electrodes over extended (long-term) cycling.

Cellulose(CMK-3/S)CB freestanding electrode and CMK-3/S electrode are shown in Fig. 4c. The Coulombic efficiency in each charge/discharge cycle is also plotted. The Cellulose(CMK-3/S)CB and CMK-3/S electrodes delivered an initial capacity of ~ 959 and ~ 961 mA h g^{-1} at 0.5 C, respectively. Interestingly, after 300 cycles, the reversible capacity of the Cellulose(CMK-3/S)CB freestanding electrode remains at around ~ 660 mA h g^{-1} with a Coulombic efficiency of around 99%, demonstrating a capacity decay rate of only ~ 0.12% per cycle. By contrast, the discharge capacity of CMK-3/S electrode changes from ~ 961 mA h g^{-1} to ~ 338 mA h g^{-1} with a capacity decay rate as high as ~ 0.35% per cycle after 300 cycles. This reduced capacity decay of the Cellulose(CMK-3/S)CB freestanding electrode is due to the fact that the sulfur has been confined effectively by the core-shell structure. The soft nature of cellulose could also provide sufficient space to accommodate the large volume change of sulfur during cycling. During the charge and discharge processes, sulfur has been protected by the cellulose shell, which will alleviate the dissolution of the soluble lithium polysulfides. It should be noted that the mesoporous structure of CMK-3 solely is not enough to prevent sulfur loss in the CMK-3/S composite electrode. In Fig. 4d and e, we have analyzed and plotted the high plateau (around 2.2 V) and the low plateau (around 2.0 V) capacity contributions to the total discharge capacity over extended cycling of the Cellulose(CMK-3/S)CB and CMK-3/S electrodes. The high plateau capacities at different cycle numbers (Fig. 4d) for the Cellulose(CMK-3/S)CB freestanding

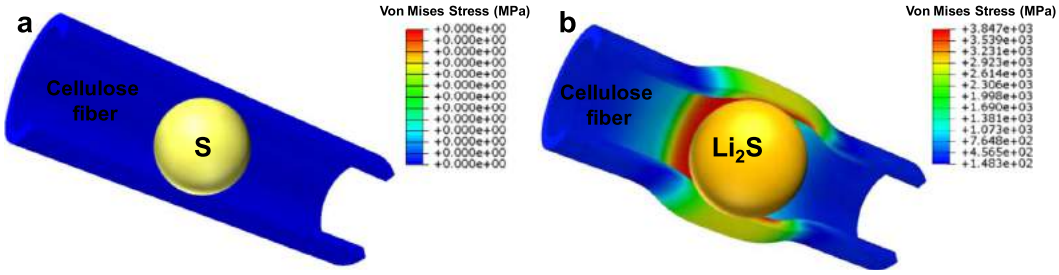

Fig. 5. Schematic illustration of the stress (Von Mises stress) of a Cellulose/S coaxial structure. **a**) Before lithiation and **b**) after lithiation.

electrode are much more stable as compared to the CMK-3/S electrode due to physical confinement brought by the coaxial nanocable structure of the cellulose tube,. We also found that the low plateau capacity (which corresponds to conversion from lithium polysulfides to lithium sulfide) for the Cellulose(CMK-3/S)CB freestanding electrode is also more stable (Fig. 4e), which confirms that the diffusion of lithium polysulfides are effectively suppressed by the cellulose shell.

The large volumetric expansion of sulfur could be up to ~ 80% after lithiation (Li_2S), which will also cause stress concentration inside the tube. In order to have a better understanding of the benefits of using cellulose fiber as a soft substrate to confine sulfur volume expansion after lithiation, we carried out a detailed finite element analysis to calculate the Von Mises stress distribution in the cellulose hollow fiber (Fig. 5) and that in a rigid matrix (such as carbon nanotube, Supporting information, Fig. S6). The Von Mises stress (σ_v) is given by:

$$\sigma_v^2 = \frac{1}{2}[(\sigma_{11} - \sigma_{22})^2 + (\sigma_{22} - \sigma_{33})^2 + (\sigma_{33} - \sigma_{11})^2] \quad (1)$$

where σ is the Cauchy stress, which can be written as follows, based on the assumption of linear elasticity:

$$\sigma_{ij} = C_{ijkl}\varepsilon_{kl} \quad (2)$$

$$C_{ijkl} = \frac{E}{3(1-2\upsilon)}\delta_{ij}\delta_{kl} + \frac{E}{2(1+\upsilon)}(\delta_{ik}\delta_{jl} + \delta_{il}\delta_{jk} - \frac{2}{3}\delta_{ij}\delta_{kl}) \quad (3)$$

here, ε is the infinitesimal strain, C is a constant fourth-order stiffness tensor which is determined by the material properties Young's Modulus (E) and Poisson's ratio (υ), and δ is the Kronecker delta (i, j, k, lϵ {1, 2, 3}). From the finite element modeling, it is evident that the maximum stress in the rigid carbon nanotube is two orders of magnitude (10^5 MPa) larger than that (10^3 MPa) in the cellulose fiber hollow structure after sulfur is converted to lithium sulfide, while the deformation in both case are at the same level (Supporting information, Fig. S7). This implies: 1) it is easier for the carbon nanotube to reach its limit of elasticity, causing plastic deformation and breaking the matrix structure under large stress and 2) sulfur could easily escape from the open-end of the nanotube after its lithiation which will lead to loss of sulfur and resultant decay of capacity. Therefore, comparing to rigid encapsulants such as carbon nanotubes, the soft cellulose material can better confine and trap sulfur, while also reducing stress concentration and structural degradation.

4. Conclusion

As a proof-of-concept demonstration, we have developed a free-standing Li-S battery electrode by using an inside-out synthesis method to encapsulate sulfur. The sulfur composite has been directly wrapped in the cellulose structure during the electrospinning process without any post processing or thermal treatment. Electrochemical tests indicate that Cellulose(CMK-3/S)CB fibers with the core-shell structure suppress sulfur and lithium polysulfide dissolution into the electrolyte. The soft nature of cellulose allows the structure to accommodate the large volume change of sulfur during cycling, without large stress build-up. This has been demonstrated by the electrode cycling performance; after 300 discharge and charge cycles, the reversible capacity of the Cellulose(CMK-3/S)CB freestanding electrode still remains at around 660 mA h g^{-1} with a Coulombic efficiency of around 99%, demonstrating a capacity decay rate of ~ 0.12% per cycle. This work demonstrates the potential of using cellulose based core-shell structures to develop advanced electrode materials with improved electrochemical stability for Li–S batteries.

Acknowledgements

N.K. acknowledges support from the USA National Science Foundation (Awards 1435783, 1510828, 1608171) and the John A. Clark and Edward T. Crossan endowed Chair Professorship at the Rensselaer Polytechnic Institute.

Appendix A. Supplementary material

Supplementary data associated with this article can be found in the online version at doi:10.1016/j.ensm.2018.08.019.

References

[1] P.G. Bruce, S.A. Freunberger, L.J. Hardwick, J.-M. Tarascon, Nat. Mater. 11 (2012) 19–29.
[2] Z.W. Seh, Y. Sun, Q. Zhang, Y. Cui, Chem. Soc. Rev. 45 (2016) 5605–5634.
[3] D.-W. Wang, Q. Zeng, G. Zhou, L. Yin, F. Li, H.-M. Cheng, I.R. Gentle, G.Q.M. Lu, J. Mater. Chem. A 1 (2013) 9382–9394.
[4] G. Zhou, E. Paek, G.S. Hwang, A. Manthiram, Nat. Commun. 6 (2015) 7760.
[5] Y. Qiu, G. Rong, J. Yang, G. Li, S. Ma, X. Wang, Z. Pan, Y. Hou, M. Liu, F. Ye, W. Li, Z.W. Seh, X. Tao, H. Yao, N. Liu, R. Zhang, G. Zhou, J. Wang, S. Fan, Y. Cui, Y. Zhang, Adv. Energy Mater. 5 (2015) 1501369.
[6] L. Li, G. Zhou, L. Yin, N. Koratkar, F. Li, H.-M. Cheng, Carbon 108 (2016) 120–126.
[7] J. Gao, L. Li, J. Tan, H. Sun, B. Li, J.C. Idrobo, C.V. Singh, T.-M. Lu, N. Koratkar, Nano Lett. 16 (2016) 3780–3787.
[8] L. Hu, C. Dai, J.-M. Lim, Y. Chen, X. Lian, M. Wang, Y. Li, P. Xiao, G. Henkelman, M. Xu, Chem. Sci. 9 (2018) 666–675.
[9] L. Li, L. Chen, S. Mukherjee, J. Gao, H. Sun, Z. Liu, X. Ma, T. Gupta, C.V. Singh, W. Ren, H.-M. Cheng, N. Koratkar, Adv. Mater. 29 (2017), 1602734.
[10] H. Yuan, X. Chen, G. Zhou, W. Zhang, J. Luo, H. Huang, Y. Gan, C. Liang, Y. Xia, J. Zhang, J. Wang, X. Tao, ACS Energy Lett. 2 (2017) 1711–1719.
[11] X. Tao, J. Wang, C. Liu, H. Wang, H. Yao, G. Zheng, Z.W. Seh, Q. Cai, W. Li, G. Zhou, C. Zu, Y. Cui, Nat. Commun. 7 (2016).
[12] H.J. Peng, Z.W. Zhang, J.Q. Huang, G. Zhang, J. Xie, W.T. Xu, J.L. Shi, X. Chen, X.B. Cheng, Q. Zhang, Adv. Mater. 28 (2016) 9551–9558.
[13] J. Liu, M. Wang, N. Xu, T. Qian, C. Yan, Energy Storage Mater. 15 (2018) 53–64.
[14] C. Jin, O. Sheng, W. Zhang, J. Luo, H. Yuan, T. Yang, H. Huang, Y. Gan, Y. Xia, C. Liang, J. Zhang, X. Tao, Energy Storage Mater. 15 (2018) 218–225.
[15] J. Liu, T. Yang, D.-W. Wang, G.Q. Lu, D. Zhao, S.Z. Qiao, Nat. Commun. 4 (2013) 2798.
[16] G. Zhou, Y. Zhao, A. Manthiram, Adv. Energy Mater. 5 (2015), 1402263.
[17] L. Xiao, Y. Cao, J. Xiao, B. Schwenzer, M.H. Engelhard, L.V. Saraf, Z. Nie, G.J. Exarhos, J. Liu, Adv. Mater. 24 (2012) 1176–1181.
[18] J. Zhang, H. Huang, J. Bae, S.H. Chung, W. Zhang, A. Manthiram, G. Yu, Small Methods 2 (2018), 1700279.
[19] P. Simon, Y. Gogotsi, Nat. Mater. 7 (2008) 845.
[20] Y. Lu, S.C. Chen, Adv. Drug Deliv. Rev. 56 (2004) 1621–1633.
[21] Y. Yao, N. Liu, M.T. McDowell, M. Pasta, Y. Cui, Energy Environ. Sci. 5 (2012) 7927–7930.
[22] J. Zhang, Z. Liu, Q. Kong, C. Zhang, S. Pang, L. Yue, X. Wang, J. Yao, G. Cui, ACS Appl. Mater. Interfaces 5 (2013) 128–134.

[23] S.S. Jeong, N. Böckenfeld, A. Balducci, M. Winter, S. Passerini, J. Power Sources 199 (2012) 331–335.
[24] J. Cheng, L.T. Zhang, Int. J. Comput. Methods 15 (2018) 1850028.
[25] A.K. Bledzki, J. Gassan, Prog. Polym. Sci. 24 (1999) 221–274.
[26] K. Shanmuganathan, J.R. Capadona, S.J. Rowan, C. Weder, J. Mater. Chem. 20 (2010) 180–186.
[27] R.H. Baughman, A.A. Zakhidov, W.A. de Heer, Science 297 (2002) 787–792.
[28] M. Miao, J. McDonnell, L. Vuckovic, S.C. Hawkins, Carbon 48 (2010) 2802–2811.
[29] L. Hou, W.M.R.N. Udangawa, A. Pochiraju, W. Dong, Y. Zheng, R.J. Linhardt, T.J. Simmons, ACS Biomater. Sci. Eng. 2 (2016) 1905–1913.
[30] Y. Zheng, J. Miao, N. Maeda, D. Frey, R.J. Linhardt, T.J. Simmons, J. Mater. Chem. A 2 (2014) 15029–15034.
[31] D. Baskaran, J.W. Mays, M.S. Bratcher, Chem. Mater. 17 (2005) 3389–3397.
[32] R.G. Zhbankov, S.P. Firsov, D.K. Buslov, N.A. Nikonenko, M.K. Marchewka, H. Ratajczak, J. Mol. Struct. 614 (2002) 117–125.
[33] M. Yu, R. Li, Y. Tong, Y. Li, C. Li, J.-D. Hong, G. Shi, J. Mater. Chem. A 3 (2015) 9609–9615.
[34] L. Li, L. Huang, R.J. Linhardt, N. Koratkar, T. Simmons, Sustain. Energy Fuels 2 (2018) 422–429.
[35] B. Abderrahim, E. Abderrahman, A. Mohamed, T. Fatima, T. Abdesselam, O. Krim, World J. Environ. Eng. 3 (2015) 95–110.
[36] C. Hampton, D. Demoin, R.E. Glaser, 2010. Available from ⟨https://faculty.missouri.edu/~glaserr/8160f10/A03_Silver.pdf⟩.
[37] C. Zu, A. Manthiram, Adv. Energy Mater. 3 (2013) 1008–1012.
[38] J. Miao, F.-X. Xiao, H.B. Yang, S.Y. Khoo, J. Chen, Z. Fan, Y.-Y. Hsu, H.M. Chen, H. Zhang, B. Liu, Sci. Adv. 1 (2015).
[39] K. Xu, X. Liu, J. Liang, J. Cai, K. Zhang, Y. Lu, X. Wu, M. Zhu, Y. Liu, Y. Zhu, G. Wang, Y. Qian, ACS Energy Lett. 3 (2018) 420–427.
[40] Z. Deng, Z. Zhang, Y. Lai, J. Liu, J. Li, Y. Liu, J. Electrochem. Soc. 160 (2013) A553–A558.
[41] L. Li, S. Basu, Y. Wang, Z. Chen, P. Hundekar, B. Wang, J. Shi, Y. Shi, S. Narayanan, N. Koratkar, Science 359 (2018) 1513–1516.
[42] R. Elazari, G. Salitra, A. Garsuch, A. Panchenko, D. Aurbach, Adv. Mater. 23 (2011) 5641–5644.
[43] K. Yang, Q. Gao, Y. Tan, W. Tian, W. Qian, L. Zhu, C. Yang, Chem. Eur. J. 22 (2016) 3239–3244.